Computational and Theoretical Chemistry 1083 (2016) 53–63

Contents lists available at ScienceDirect

Computational and Theoretical Chemistry

journal homepage: www.elsevier.com/locate/comptc

On the search of stable, aromatic and ionic endohedral compounds of C_{28}: A theoretical study

Alan Miralrio, Luis Enrique Sansores *

Departamento de Materiales de Baja Dimensionalidad, Instituto de Investigaciones en Materiales, Universidad Nacional Autónoma de México, Apartado, Postal 70-360, México, DF 04510, Mexico

ARTICLE INFO

Article history:
Received 21 February 2016
Received in revised form 7 March 2016
Accepted 11 March 2016
Available online 16 March 2016

Keywords:
Density functional theory calculation
Endohedral fullerenes
C_{28} fullerene
Electronic structure

ABSTRACT

The $X@C_{28}$ compounds form the family of the smallest endohedral fullerenes. Currently, they consist of C_{28}, which is endohedrally doped with group-4 elements (Ti, Zr, Hf) and U. We have studied the electronic properties, equilibrium geometries, binding energies and other properties of several $X@C_{28}$ at the PBE/def2-TZVP level. These were compared with the tetraanion C_{28}^{4-}. For this study we have chosen elements from groups 4, 14 and Sc as endohedral dopants for being many of them tetravalent. In addition, we studied by the first time the entire group-10 (Ni, Pd and Pt) as endohedral dopant of C_{28}. To elucidate the stability of these ionic compounds, we have studied their binding energies. Our results show that a big positive binding energy is necessary but not enough to determine the stability of these endohedral fullerenes. We propose that a HOMO–LUMO gap around 2 eV results in less reactive compounds, property only shown by group-4 compounds. Some compounds have aromatic character in all rings according with their $NICS(0)_{iso}$ and reparametrized HOMA indexes. In addition, the charge distribution have been studied with NBO and Hirshfeld population analysis as well as electrostatic potential maps in order to find similarities between them and that shown by the tetraanion C_{28}^{4-}. The most stable compounds are the group-4 $X@C_{28}$ which form compounds: energetically favorable, less reactive, ionic and aromatic. Our results are compared with available experimental information about the formation of these compounds.

1. Introduction

During the same year of the discovery of fullerene C_{60} [1], it was found that fullerenes has the capacity to contain other species inside [2] (atoms, molecules or clusters [3–5]). These internally doped fullerenes are known as endohedral fullerenes (**EF**s). The most common EFs are the endohedral metallofullerenes (**EMF**s) that contain lanthanide atoms [3], encapsulated inside C_{60}, or larger cages [5].

An important difference between hollow fullerenes and EFs is that EFs can violate the isolated pentagon rule (**IPR**) [3–5]; this rule predicts that most stable isomer, from all possible, has its pentagonal rings solely surrounded by hexagonal rings. This excludes the isomers with two or more adjacent pentagonal rings. However, EFs can violate the IPR [6], and many of their cages show fused pentagonal rings [3–5]. The stability of this kind of compounds can be explained by the donation of charge from the metal atoms to the pentagonal fused rings [3]. Many EMFs are formed by large fullerenes (C_{60} and higher) [5], although there exist a few EFs that enclose atoms inside a small cage. The smallest EFs known form the $X@C_{28}$ family, discovered in the synthesis of the $U@C_{28}$ by laser evaporation [7] of graphite-UO_2. Unlike most common EMFs, the $U@C_{28}$ encloses an actinium atom inside an unstable cage in its isolated form.

Although theoretically the fullerene C_{20} is the smallest hollow fullerene possible [8], it's a highly strained structure that hinders its formation [9] and a ring geometry is preferred [9]. Experimentally, the smallest fullerene is the C_{28}, detected for the first time in the mass spectra obtained from the pulsed-laser evaporation of a lanthanum-impregnated graphite rod [10]. The C_{28} was theoretically described [11] as a cage with tetrahedral symmetry. Apart from the T_d-C_{28}, it is possible to obtain another isomer [12]: the D_2-C_{28}. Both isomers are highly strained non-IPR structures [12], and their states are quintet and singlet, respectively. According with several theoretical results [13,14], the most favorable isomer is the quintet T_d-C_{28}.

The T_d-C_{28} structure is formed by four hexagonal rings in the faces and four groups of triply fused pentagonal rings (Fig. 1) called

* Corresponding author.
E-mail addresses: miralrio@ciencias.unam.mx (A. Miralrio), sansores@unam.mx (L.E. Sansores).

http://dx.doi.org/10.1016/j.comptc.2016.03.010
2210-271X/

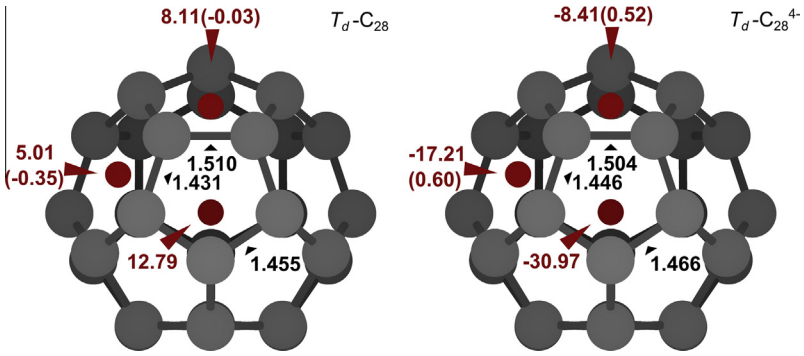

Fig. 1. Structures of the T_d-C_{28} fullerene. Neutral quintet state (left) and tetraanion in singlet state (right). Both calculated at the DFT level PBE/def2-TZVP. Distances (black) are in Å, the NICS(0)$_{iso}$ values (red) calculated with GIAO-PBE/LANL2DZ in ppm, HOMA values in brackets. (For interpretation of the references to color in this figure legend, the reader is referred to the web version of this article.)

5:5:5 vertices. On the other hand, in agreement with experiments [10] theoretical studies predicted the instability of the C_{28} compared with the largest fullerenes [15]: C_{60} and C_{70}. The tendency to form large fullerenes arises from the possibility of obtaining structures that follow the IPR rule [11]. Additionally, it has been shown that the stability and HOMO–LUMO gap increases consistently with the number of carbon atoms [15]. Recent studies also show that the C_{28} is a tetravalent fullerene [7,8] that can be stabilized by an appropriate doping [16]. According with nucleus-independent chemical shift (**NICS**) calculations performed with the gauge-independent atomic orbital (**GIAO**) method, the neutral C_{28} shows non-aromatic or weakly aromatic character [16,17] in its rings. Oppositely, the tetraanion C_{28}^{4-} shows increased aromatic character in its rings [16,17], improving the stability of the whole cage [16,17]. Moreover, the tetraanion follows a $2(N+1)^2$ rule for spherical aromaticity [17] with a 32-electron π-conjugation. This agrees well with the model of a hollow tetravalent "superatom" that can be stabilized from both inside and outside by chemical bonding [18].

Doping is a way to obtain more stable derivatives of C_{28}. The synthesis of U@C_{28} demonstrated the possibility of endohedral stabilization [7], producing the most abundant species in that synthesis, thus, it exist the possibility of obtaining stable [16] endohedral-, exohedral- or heterofullerenes. In addition, other endohedral compounds [19,20] which satisfy the 32-electron principle have been proposed. The problem arises from the requirement of the C_{28} to pair its four unpaired electrons to form a closed-shell compound similar to the tetraanion C_{28}^{4-}. Studies have suggested that the hydrogenation of their four vertices can produce a quite stable [8] $C_{28}H_4$; other exohedral derivatives have also been proposed [16]. Furthermore, the endohedral stabilization by electropositive metallic atoms has been studied [21]. According with the ionic model, an electropositive atom with oxidation state 4+ can donate enough charge to the fullerene to stabilize it, forming an ionic compound $M^{4+}@C_{28}^{4-}$ [7,21]. In addition, X-ray photoelectron spectroscopy experiments proved during the U@C_{28} synthesis that the U atom has a formal 4+ oxidation state [7]. Today, other three endohedral M@C_{28} complexes have been synthesized, all with group-4 atoms (Ti, Zr and Hf) [7,22]. Other elements have been proposed theoretically [19,21], but experimentally, only four endohedral fullerenes are considered to be stable [7,22]: M@C_{28} (M = U, Ti, Zr and Hf). For that reason, the stability of other possible endohedral fullerenes needs to be studied. This work describes by first time the entire group-10 (Ni, Pd and Pt) as endohedral dopant of C_{28}. The study is done in comparison with group-4 endohedral compounds, as well as group-14 and Sc. Geometric, electronic, aromatic and others properties are discussed.

2. Computational details

We have obtained the lowest stable energy geometries of several endohedral fullerenes X@C_{28}, where X is an endohedral atom belonging to group-4 (Ti, Zr, Hf), group-10 (Ni, Pd, Pt), group-14 (Si, Ge, Sn Pb) or Sc. These calculations were carried out within the DFT methodology, using the generalized gradient approximation (**GGA**) functional of Perdew, Burke and Ernzerhof [23] (**PBE**). For the basis we used the triple-ζ valence basis set with one set of polarization functions def2-TZVP [24], which uses an effective core potential (**ECP**) with 28 or 60 electrons for 5p and 6p block elements. The method PBE/def2-TZVP was used in the *Turbomole 6.5* package [25] to optimize the proposed structures with the finest grid size available m5. These optimizations started from several proposed structures with the endohedral atom located at different positions inside the T_d-C_{28}, with the lowest multiplicity and the next one. We report the lowest energy structures. Furthermore, we used the PBE/def2-TZVP method to obtain the natural bond orbitals (**NBO**) and density based (Hirshfeld) charges and vibra-

Table 1
Comparison between experimental and theoretical bond lengths and radius of C_{60} fullerene. The error refers to the mean absolute percentage error obtained.

Method	Single bond (Å)	Double bond (Å)	Radius (Å)	Error (%)
Experimental [27]	1.4586	1.4011	3.5620	–
HF/6-31G(d) [28]	1.4486	1.3732	3.5224	1.28
B3LYP/6-31G(d) [28]	1.4535	1.3952	3.5497	0.37
MP2/6-31G(d) [28]	1.4469	1.4072	3.5500	0.53
PBE/6-31G(d)	1.4568	1.4050	3.5638	0.15
PBE/6-311G(d)	1.4543	1.4014	3.5566	0.16
PBE/def2-TZVP	1.4524	1.3987	3.5511	0.30
M06-2X/6-31G(d)	1.4515	1.3880	3.5401	0.68
M06-2X/6-311G(d)	1.4505	1.3855	3.5363	0.80
M06-2X/def2-TZVP	1.4478	1.3825	3.5295	1.00

tional frequencies; we only considered structures with all their vibrational frequencies real. Lowest unoccupied molecular orbitals (**LUMO**), highest occupied molecular orbitals (**HOMO**), HOMO-1, electrostatic potential maps (**ESP**) and others, were plotted using the *Gaussview 5* program [26]. ESP was mapped over isosurfaces of 0.1 a.u. electron density.

To test our methodology, we used the neutral I_h-C_{60} fullerene to compare the PBE/def2-TZVP method with other calculations [28] and experimental results [27,29]. First of all, we optimized the I_h-C_{60} fullerene with the GGA functional PBE and the hybrid meta-GGA functional M06-2X, together with the polarized double-ζ basis 6-31G(d), the polarized triple-ζ 6-311G(d) and the basis def2-TZVP. Table 1 shows the error (mean absolute percentage error) obtained in the comparison between radius, single bond length and double bond length measured in I_h-C_{60} by electron diffraction experiments [27] and the proposed methods, as well as other calculations [28]. Those calculations were done with various methodologies: Hartree–Fock theory (**HF**), second order Møller–Plesset perturbation theory (**MP2**) as well as DFT with the hybrid functional B3LYP, all with the polarized double-ζ basis set 6-31G(d). The PBE functional obtained the smallest errors (Table 1) followed by the B3LYP/6-31G(d) method. The meta-GGA functional and the HF method gave the largest errors. In this geometrical comparison, the PBE/def2-TZVP method obtained an error of 0.30%. Comparison with the geometrical parameters measured by nuclear magnetic resonance (**NMR**) experiments [29] reduces the error to 0.21% for the PBE/def2-TZVP method (Supplementary information).

Comparing with 14 experimental vibrational [28] frequencies of C_{60} measured by the Fourier transform infrared spectroscopy (**FT-IR**) technique. The PBE/def2-TZVP method obtained the best fit, with an error of 1.48% (Table 2), the lowest value obtained. The proposed method was followed by the PBE/6-311G(d) and B3LYP/6-31G(d) methods, with 1.60% and 1.93% of error respectively. Similarly to the geometrical case, the functional M06-2X and Hartree Fock calculations gave the worst results with the largest errors (Table 2).

According with our comparison, independently of the basis set employed, the GGA functional PBE gave the most accurate geometrical parameters and vibrational frequencies in the comparison with experimental results. To test the energetic properties predicted for C_{60} by the PBE/def2-TZVP method we compared with experimental values: the electron affinity (**EA**) calculated as 2.6719 eV underestimates by 0.43% the 2.6835 eV value measured by laser photoelectron spectroscopy [30], the ionization energy (**IE**) calculated as 7.4 eV underestimates by 2.63% the IE measured with electron impact techniques [31] (7.6 eV). In conclusion, we used the method PBE/def2-TZVP because we can obtain more accurate results in comparison with other DFT methods, as well as HF and MP2 calculations. To determine the stability of the studied compounds, we calculated the binding energy (**BE**) as: *Binding Energy* = $E(C_{28}) + E(X) - E(X@C_{28})$. The term $E(C_{28})$ refers to the total energy of the isolated neutral C_{28} in singlet state optimized at the PBE/def2-TZVP level. The second term $E(X)$ is the energy of the endohedral atom X in its atomic ground state. Finally $E(X@C_{28})$ is the energy of the endohedral compound fully optimized (do not confuse with the interaction energy that uses the energy of the parts in the geometry of the compound). We choose this definition to be consistent with that employed previously for the analysis of binding energies in other $X@C_{28}$ compounds [21,32,33]. According with our definition, a positive binding energy denotes a stable compound in comparison with the C_{28} and the endohedral atom. On the contrary, a negative value denotes an unstable compound in comparison with the parts that form it. The most common definition of BE uses the negative of this amount.

Table 2
Comparison between 14 experimental and theoretical vibrational frequencies of C_{60} fullerene. The error refers to the mean absolute percentage error obtained.

Method	Error (%)
HF/6-31G(d) [28]	9.42
B3LYP/6-31G(d) [28]	1.93
PBE/6-31G(d)	1.96
PBE/6-311G(d)	1.60
PBE/def2-TZVP	1.48
M06-2X/6-31G(d)	3.11
M06-2X/6-311G(d)	2.61
M06-2X/def2-TZVP	3.02

Finally, for the analysis of aromatic properties we calculated $NICS(0)_{iso}$ values by obtaining the nuclear magnetic resonance shielding tensor with the GIAO method. We took the negative of its isotropic value calculated at the centroid of several pentagonal and hexagonal rings. A negative $NICS(0)_{iso}$ value denotes aromatic character. On the contrary, a positive value denotes an antiaromatic character and non-aromatic if the value is close to zero [16,34]. To perform these calculations we used the PBE functional in combination with the effective core potential (**ECP**) and basis set LANL2DZ [35] into the Gaussian 09 program [36]. The ghost atom required for the calculation was put at the centroid of each ring analyzed. Both def2-TZVP and LANL2DZ ECPs basis sets include scalar relativistic effects for heavy elements. For comparison, we calculated the harmonic oscillator model of aromaticity (HOMA) index of the same rings analyzed with $NICS(0)_{iso}$. The HOMA indices were carried out with a special reparameterization (R_{opt} = 1.46546 Å and α = 1103.38 Å^{-2}) using the generalized formulation proposed by Krygowski [37]. Our parameterization takes into account the aromaticity of the tetra anion C_{28}^{4-} and the weak aromatic or non-aromatic behavior of the neutral species C_{28}. The parameters were obtained putting the tetra anion's C_{28}^{4-} largest bond length R(s) = 1.504 Å and the shortest bond length R(d) = 1.446 Å calculated at the PBE/def2-TZVP level for the aromatic reference T_d-C_{28}^{4-} (detailed below) (Fig. 1) into the Krygowski's parameterization formulae [37]. If HOMA equals 1 means that each bond length in the ring equals the optimal bond length and the ring is fully aromatic [37]. On the contrary, a negative HOMA denotes an antiaromatic ring character and a value close to zero a non-aromatic [37].

3. Results and discussion

3.1. Isolated C_{28} neutral and tetra anion

To understand the formation of the endohedral fullerenes $X@C_{28}$, we started calculating the optimized structures of the neutral C_{28} and its tetra anion C_{28}^{4-} at the DFT level PBE/def2-TZVP. It is known that the C_{28} has two isomers [12] with symmetries T_d and D_2. In agreement with other calculations [13,14], the most favorable isomer energetically is the T_d-C_{28} in its open-shell ground state $^5A_2$ (quintuplet), with an energy difference of 0.774 eV with respect to the singlet D_2-C_{28} isomer. Due to symmetry reasons, the T_d-C_{28} has only three different bond lengths (Fig. 1). The 5:5 bonds that connect two pentagonal rings have bond length 1.431 Å. The 5:6 connects a pentagonal ring with a hexagonal ring has bond length 1.455 Å, and the 6:6 bonds between two hexagonal rings length 1.510 Å. Our structural parameters agree very well with recent calculations [33] at the level ROMP2/6-31G(d), which obtained bond lengths of 1.434 Å, 1.440 Å and 1.499 Å for the 5:5, 5:6, and 6:6 bonds, respectively; our results show only 0.7% difference. On the contrary, the tetra anion C_{28}^{4-} shows a closed-shell state $^1A_1$ (singlet) with the same T_d symmetry (Fig. 1). The tetra anion increases its bond lengths to 1.446 Å and 1.466 Å for

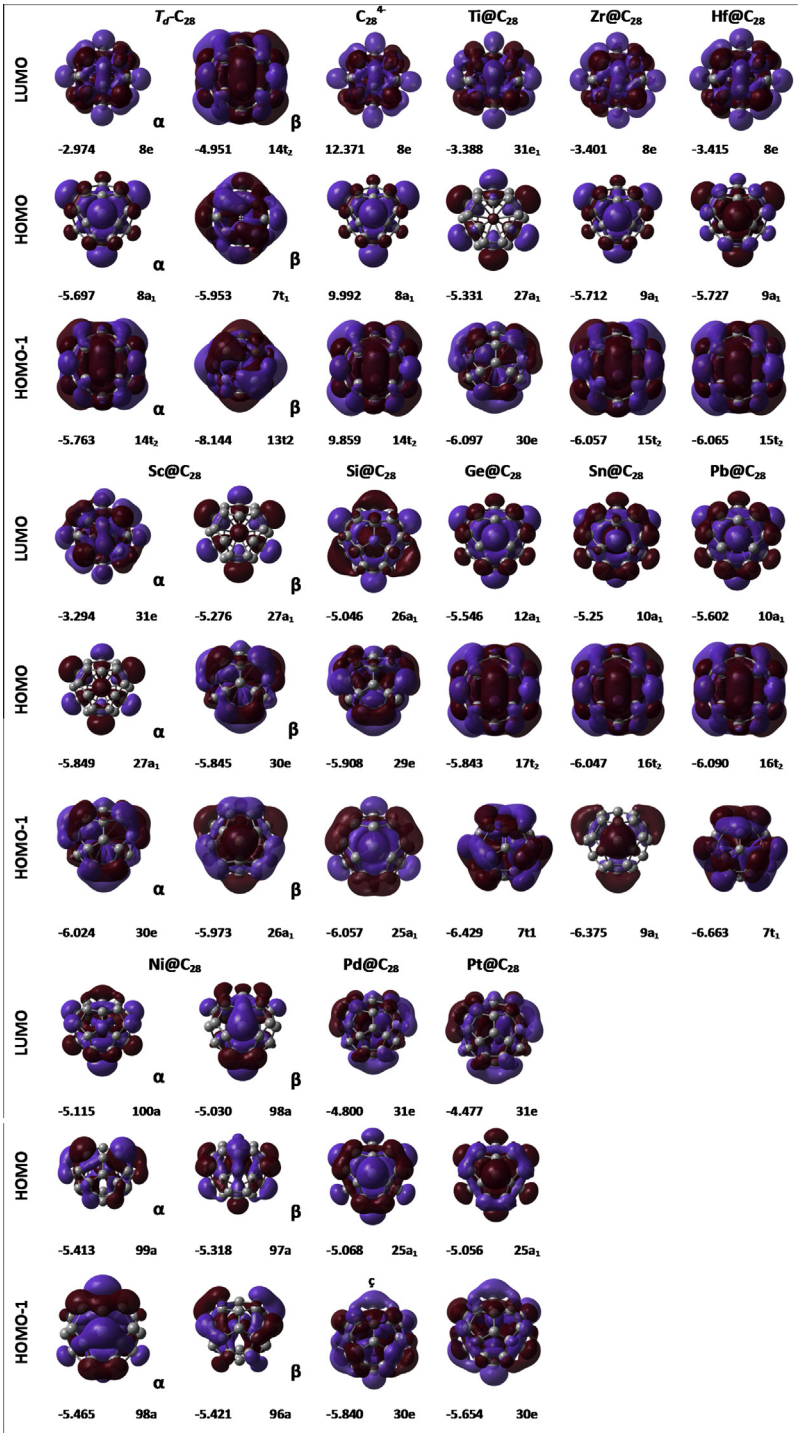

Fig. 2. HOMO, HOMO-1 and LUMO of all X@C_{28}. Degenerated states are shown as the superposition of orbitals. Orbital label and related energies in eV annotated below.

the 5:5 and the 5:6 bonds, but 6:6 bonds are reduced to 1.504 Å. It is remarkable that the difference between the largest and the shortest bond length was reduced from 0.079 Å (in the neutral case) to 0.058 Å for the charged species. It is clear that it is a consequence of a more aromatic character of the C_{28}^{4-}.

The molecular orbitals that belong to the neutral C_{28} have an HOMOα, which corresponds to the single degenerate state $8a_1$, due to (Fig. 2) *p* orbitals at the 5:5:5 vertices and a contribution extended over the fullerene's inner part. HOMOβ shows π orbitals over the fullerene without contributions at the 5:5:5 vertices. Both LUMOβ and HOMO-1α correspond to the triply degenerate state $14t_2$ which are π bonding orbitals extended over the whole fullerene and *p* orbitals at the 5:5:5 vertices. HOMO-1β shows π orbitals over the whole fullerene. LUMOα shows a mix of π bonding orbitals and *p* orbitals, without contributions at the vertices. The HOMO–LUMO gap has a small value of 0.746 eV and was calculated as the energy difference between HOMOα and LUMOβ. This small amount agrees with its instability and with the relationship between small gap and high reactivity [38]. The symmetry and shape of the HOMO and LUMO of the tetra anion C_{28}^{4-} correspond to the alpha unpaired orbitals of neutral C_{28} (Fig. 2). The HOMO–LUMO gap increased to 2.379 eV. The bigger gap corresponds to

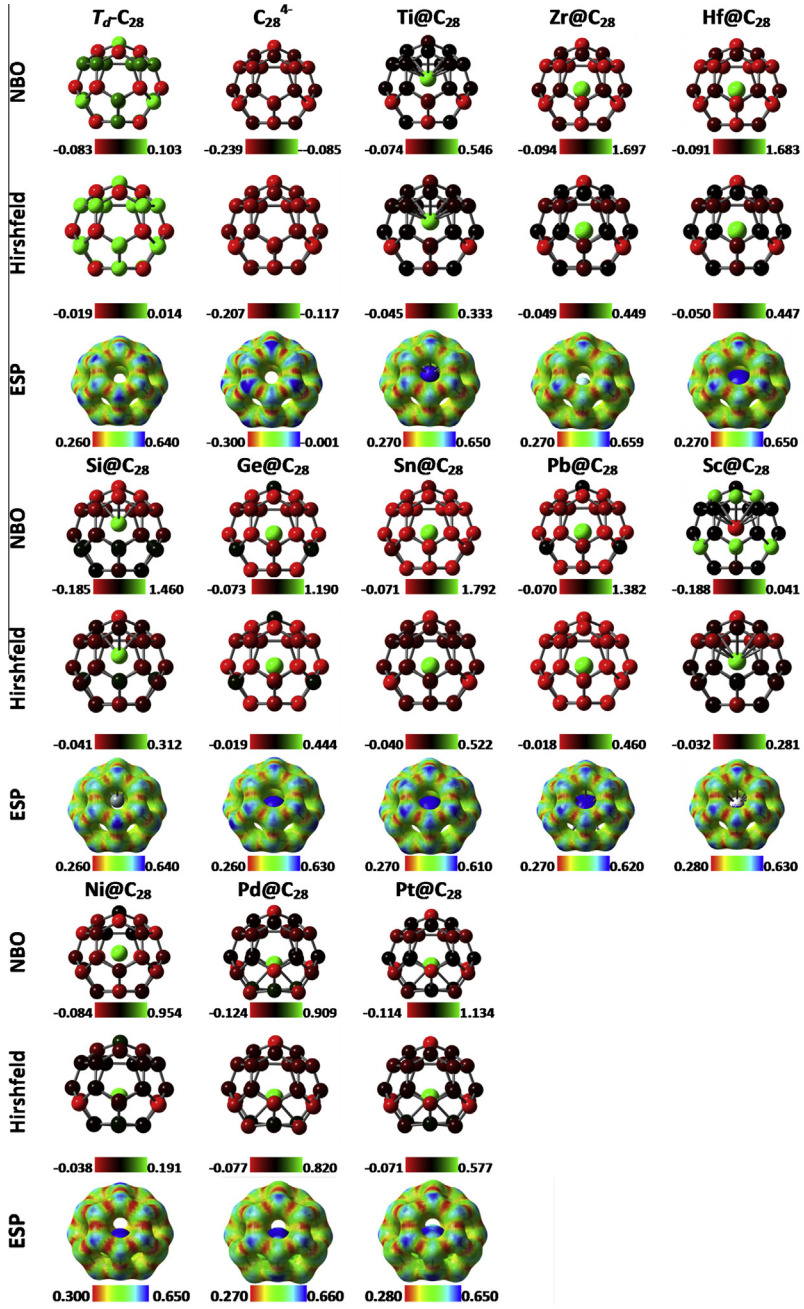

Fig. 3. NBO, Hirshfeld charge distributions and ESP map of all X@C_{28}. Ranges annotated in a.u. and ESP mapped over the isosurface with electron density of 0.1 a.u.

the filling and pairing of these orbitals. The increased stability is due to this increment in the gap.

According with the NBO and Hirshfeld charge distributions (Fig. 3). The neutral C_{28} has its most positive charges located at the 5:5:5 vertices, with values 0.103 and 0.014 respectively. In addition, the ESP map shows (Fig. 3) that the vertices are the most positive potential compared with other regions near the carbon atoms. Moreover, these vertices are the most prominent reactive sites [18]. This charge deficiency at the vertices, along with available bonding orbitals, explains [8] the hydrogen atoms located at the vertices of the exohedral $C_{28}H_4$. On the contrary, the ESP and charges in the tetra anion C_{28}^{4-} show a redistribution of charges (Fig. 3) with an important charge transferred to the vertices; with values −0.239 and −0.207 for NBO and Hirshfeld respectively. These are the most negative values obtained in both cases.

We characterized the systems that are being studied with the $NICS(0)_{iso}$ and HOMA values to study their aromatic properties. According with their large positive $NICS(0)_{iso}$ values calculated at the centroid of them and at the fullerene center with the GIAO-PBE/LANL2DZ method (Fig. 1); the neutral C_{28} fullerene shows an antiaromatic behavior in all their rings. So, the C_{28} instability can be understood as a consequence of the antiaromatic nature of all their rings that destabilizes the whole compound. Besides, the HOMA values calculated (Fig. 1) indicate a weak antiaromatic or non-aromatic character in its hexagonal rings and non-aromatic in the pentagonal. Both values agree with the $NICS(0)_{iso}$ analysis reported previously by other group calculated with the GIAO-B3LYP/6-31G(d) method [39]. In contrast, the tetra anion C_{28}^{4-} have negative $NICS(0)_{iso}$ values (Fig. 1) which indicates an aromatic behavior of its rings and whole cage. In addition, the HOMA values

indicate an aromatic character with their positive values more close to 1. As discussed above, the C_{28}^{4-} is considered fully aromatic [16,17,39].

3.2. Geometrical properties of X@C_{28}

Firstly, we studied the X@C_{28} with group-4 elements. In addition to U, that group forms the unique endohedral compounds of C_{28} whose synthesis has been reported [7,21]. **Ti@C_{28}** was obtained in singlet state and with C_{3v} symmetry (Table 3). The Ti is located off-center, with a displacement of 0.460 Å in direction of a 5:5:5 vertex (Table 3). This agrees well with other calculations [21] that localize the titanium atom 0.487 Å off-center and other calculations [22,33]. Compared with the C_{28} (Fig. 1), the 5:5 and 5:6 bond lengths near the Ti atom are increased to 1.464 Å and 1.486 Å. On the contrary, the 6:6 bond lengths are decreased to 1.498 Å. In agreement with previous works [21] **Zr@C_{28}** has T_d symmetry and singlet state (Table 3). The Zr atom is located at the fullerene's center. Similarly to the C_{28}^{4-}, the 5:5 and 5:6 bond lengths increased to 1.458 Å and 1.462 Å, while the 6:6 bonds decrease to 1.502 Å with respect to the geometry of the neutral C_{28}. The difference between the shortest and longest bond length is reduced to 0.044 Å. Similarly to Zr@C_{28}, the **Hf@C_{28}** has T_d symmetry and singlet state (Table 3), its geometry is considerably similar to Zr@C_{28}, with bond lengths 1.459 Å, 1.463 Å and 1.503 Å, for 5:5, 5:6 and 6:6 bonds, respectively. Hf also remains on-center and the difference between bond lengths has the same value: 0.044 Å.

Group 14-elements have been studied previously by other groups [21,32]. **Si@C_{28}** has singlet state, with Si displaced off-center by 0.583 Å, in the direction of a 5:5:5 vertex (Table 3). This displacement of the endohedral species decreases its symmetry to the C_{3v} group. The 5:6 bond nearest to the Si is increased to 1.455 Å, and also the nearest 5:5 bond is increased to 1.475 Å. On the contrary, the 6:6 bonds are decreased to 1.495 Å. This structure disagrees with previous calculations done at the Hartree–Fock [21] and LDA [32] levels whose structures have T_d symmetry with Si located on-center and in triplet state. Our structure was obtained departing from the potential energy surface (**PES**) scan (calculated at a rigid geometry and with the PBE/def2-TZVP level). We obtained that the Si on-center is an unstable point of the PES. Also, according with our calculations, the singlet state is the lowest energy state by energy difference of 0.430 eV with respect to the triplet state. The **Ge@C_{28}** has been obtained in singlet state with T_d symmetry and the endohedral Ge located on-center (Table 3). Furthermore, compared with the T_d-C_{28} geometry, the 5:5, 5:6 and 6:6 bonds are increased to 1.457 Å, 1.467 Å, and 1.515 Å. The difference between bond lengths has the same value of the tetra anion's case 0.058 Å. Similarly to the Ge@C_{28}, the optimized structure of **Sn@C_{28}** has the Sn located on-center in singlet state and with T_d symmetry (Table 3). Their 5:5 bonds are increased to 1.468 Å, and the 5:6 increased to 1.473 Å. Curiously, the 6:6 bonds length (1.511 Å) remains practically equal to the 6:6 bonds of C_{28}. In this case the difference between bond lengths is pretty similar to group-4 EFs, with a value of 0.043 Å. In addition, **Pb@C_{28}** is obtained as an EF in singlet state with T_d symmetry (Table 3). Similarly to Ge@C_{28} and Sn@C_{28}, the endohedral atom is located on-center (Table 3). The 5:5, 5:6 and 6:6, bond lengths increased to 1.478 Å, 1.481 Å and 1.529 Å. Compared with the hollow C_{28}, the difference between bond lengths decreased to 0.051 Å.

Group-10 behaves very different in comparison with group-4 X@C_{28}. Ni@C_{28} breaks the entire symmetry (group C_1) due to a Jahn Teller effect. The multiplicity of this system is triplet (Table 3), with an energy difference with respect to the singlet state of 1.354 eV. Unlike the systems discussed before, the endohedral Ni is located over a hexagonal ring oppose to a 5:5:5 vertex, with a displacement off-center of 0.463 Å. Similarly, **Pd@C_{28}** is obtained in singlet state and reduces the fullerene's symmetry to a C_{3v} group, and Pd is located 0.458 Å off-center (Table 3). The bond lengths of the hexagonal ring are significantly increased to 1.536 Å. In addition, **Pt@C_{28}** is obtained with C_{3v} symmetry in singlet state (Table 3). The Pt atom is displaced 0.467 Å off-center above a hexagonal ring with bond lengths of 1.551 Å.

Finally, **Sc@C_{28}** has an open-shell structure with doublet state (Table 3). Similarly to Ti@C_{28}, its symmetry is C_{3v}, and the Sc is located below a 5:5:5 vertex displaced off-center 0.255 Å which agrees with a previous HF calculation [21]. The nearest 5:5 and 5:6 bond lengths were increased to 1.460 Å, and 1.469 Å. As Ti@C_{28}, its 6:6 bond lengths were reduced to 1.501 Å.

3.3. Binding energies

From the discovery [7] of the U@C_{28}, only another three stable endohedral fullerenes X@C_{28} have been obtained [7,22], all of them containing group 4 metallic endohedral elements (X = Ti, Zr and Hf). According with these experiments [7], the relative abundances of X@C_{28}, produced in laser vaporization experiments, follow the order Ti@C_{28} ≪ Zr@C_{28} < Hf@C_{28} < U@C_{28}. Binding energies calculated for these compounds follow the same order (Fig. 4), ergo; the binding energy at the PBE/def2-TZVP level is a good indicator to study the stability of this kind of compounds. Due to the possibility of important dispersion contributions to the energy [40], a comparison between the pure PBE and the dispersion-corrected PBE-D3(BJ) [41] was done. According with our results comparison with the dispersion-corrected calculations only gives an absolute mean difference of 0.059 eV. In these systems the dispersion energy correction is very small and can be neglected and only in

Table 3
Multiplicity and symmetry group of all X@C_{28}, and off-center displacement of the X atom in Å.

X@C_{28}	M	Symmetry	Off-centre displacement (Å)
Si	1	C_{3v}	0.583
Sc	2	C_{3v}	0.255
Ti	1	C_{3v}	0.460
Ni	3	C_1	0.463
Ge	1	T_d	0.000
Zr	1	T_d	0.000
Pd	1	C_{3v}	0.458
Sn	1	T_d	0.000
Hf	1	T_d	0.000
Pt	1	C_{3v}	0.467
Pb	1	T_d	0.000

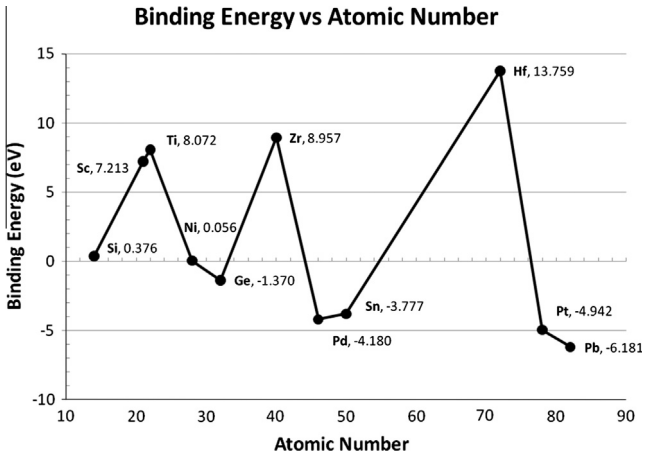

Fig. 4. Binding energy of all X@C_{28} in eV vs atomic number of their X species.

the Ni case is important. The binding energy calculated for **Ti@C_{28}** is 8.072 eV (Fig. 4) which agrees with previous LDA calculations (9.8 eV) [32] and disagrees with HF results [21] which obtained −0.8 eV. Further calculations obtained an binding energy of 9.340 eV at the R(O)MP2/6-31G(d) level of theory [33]; taking in account the basis set superposition error, the energy decreases to 7.862 eV, in agreement with our result. Similarly to Ti@C_{28}, **Zr@C_{28}** has a large positive binding energy (Fig. 4): 8.957 eV, which agrees with other calculations [21,32] (2.8 eV at the HF level and 12.9 eV with LDA). In addition **Hf@C_{28}** has positive binding energy of 13.759 eV (Fig. 4), which is the largest binding energy of all the compounds studied. This agrees with the experiments [7] that obtain Hf@C_{28} as the most abundant X@C_{28} of group-4.

With respect to the group-14 X@C_{28} compounds, **Si@C_{28}** has a small positive binding energy calculated as 0.376 eV (Fig. 4), which agrees with the LDA (1.5 eV) calculation mentioned previously [32], in disagreement with the HF value −7.8 eV [21]. The calculated binding energy (Fig. 4) is small compared with the EFs obtained in experiments. According to our definition, a positive value denotes a more stable compound compared with its components (C_{28} and X atom). Thus, the Si@C_{28} is not a very stable structure. Experiments show [22] that Si does not form endohedral compound with C_{28}. In similar way, **Ge@C_{28}** can be related to an unstable compound. Ge@C_{28} has negative binding energy, calculated as −1.370 eV (Fig. 4), which agrees with previous Hartree–Fock calculation [21] and disagrees with the positive value of 0.8 eV obtained with a LDA calculation [32]. In addition, the unfavorable binding energy agrees with the non-formation reported in experiments [22]. In the case of **Sn@C_{28}**, the binding energy was −3.777 eV (Fig. 4). This negative value indicates an unstable structure, which agrees with recent experimental observations [22] about the non-formation of this compound and other theoretical studies [21,32]. According with these studies, Si, Ge, and Sn cannot be enclosed inside a C_{28} cage [22]. These results validate our conclusions about the stability of these atoms. Finally **Pb@C_{28}** has a negative binding energy (Fig. 4) of −6.181 eV denotes that the compound must be unstable.

In the case of group-10 X@C28, **Ni@C_{28}** has binding energy calculated as 0.056 eV (Fig. 4), much smaller than that calculated for group-4 X@C_{28}. This small binding energy can be related with the non-formation of this compound [22]. All properties discussed above agree with the unique theoretical study [42] about Ni@C_{28} which obtained 0.54 eV for the binding energy at the PBE/DZP level. In this case the binding energy is increased by taking into account the dispersion interactions. Using the dispersion-corrected PBE-D3(BJ)/def2-TZVP method the binding energy increases to 0.148 eV. Anyway, the compound should be unstable. The large negative binding energy of **Pd@C_{28}** with value −4.180 eV (Fig. 4) denotes an unstable compound in agreement with experiments that show the impossibility of its formation [22]. Similarly, **Pt@C_{28}** has been predicted as an unstable compound due to its large negative binding energy, −4.942 eV (Fig. 4).

In particular, **Sc@C_{28}** has binding energy quite similar to Ti@C_{28}, with a value of 7.213 eV (Fig. 4). According with experimental information available [22,43], Sc atoms forms a lot of endohedral fullerenes, but, has not been observed in the experiments with the C_{28} cage as reported in the literature [22,43]. Our calculations agree with an energetically favorable endohedral compound. A previous HF calculation [21] obtained a positive binding energy too (1.5 eV), but those calculations do not considered the C_{3v} symmetry.

3.4. Molecular orbitals

Endohedral fullerenes doped with group-4 atoms show mainly molecular orbitals that resemble the orbitals obtained for the tetraanion C_{28}^{4-}. In particular, **Ti@C_{28}** has a double degenerated LUMO, which corresponds to the state $31e_1$. LUMO is similar to that obtained for the C_{28}^{4-} with a mix of π bonding and *p* orbitals with small contributions at the vertices. In agreement with another calculation [22], HOMO which corresponds to the single degenerated state $27a_1$ is similar to the HOMO obtained for the tetraanion, with *p* orbitals at the 5:5:5 vertices and neighboring atoms, with a small *p* contribution at the 5:5:5 vertex in line with Ti. HOMO-1 is also similar to its counterpart; it shows π bonding orbitals extended over the whole fullerene and *p* orbitals at the 5:5:5 vertices, without contributions at the atom over Ti. This orbital corresponds to the double degenerated state 30e. The HOMO–LUMO gap calculated as 1.943 eV (Fig. 5) is similar to the 2.379 eV obtained for the C_{28}^{4-}, due to the electrons transferred from the Ti to the cage. Along with the binding energy, its big HOMO–LUMO gap denotes stability due to a low reactivity. The C_{3v} symmetry and the HOMO–LUMO gap, not completely equal to the tetraanion C_{28}^{4-}, is related to a partially covalent interaction [33] between the fullerene cage and Ti atom.

Both **Zr@C_{28}** and **Hf@C_{28}** have LUMO, HOMO and HOMO-1 with the same shape and degeneration of tetraanion's orbitals (Fig. 2), corresponding with the doubly, singly and triply degenerated states 8e, $9a_1$ and $15t_2$ respectively. LUMOs show a mix of π bonding orbitals and *p* orbitals, without contributions at the vertices. In the case of Hf@C_{28}, HOMO is similar to that of the tetraanion's, with *p* orbitals at the 5:5:5 vertices and a contribution extended over the fullerene's inner part. Similarly, HOMO-1 is similar to their counterpart, showing π bonding orbitals extended over the whole fullerene and *p* orbitals at the 5:5:5 vertices. Both Zr@C_{28} and Hf@C_{28} have HOMO–LUMO gaps very close to the tetraanion's gap 2.379 eV (Fig. 5), with values 2.311 eV and 2.312 eV respectively. The first one agrees very well with the value 2.3 eV obtained [32] by Jackson et al. As discussed before, the stability in the case of X@C_{28} is due to the electronic states, similar to the orbitals of C_{28}^{4-}, which result in relatively low reactive compounds according with their HOMO–LUMO gaps.

On the contrary, group-14 X@C_{28} shows orbitals that differ from the tetraanion's orbitals. **Si@C_{28}** has HOMO and LUMO that show (Fig. 2) mainly π bonding orbitals and with some *p* at the vertices from LUMO, with small contributions at the vertex in line with Si. HOMO-1 has π bonding orbitals over the surface and *p* at all vertices. The HOMO–LUMO gap is calculated as 0.862 eV and it is smaller than the tetraanion's gap. All the other members of group-14 X@C_{28}: **Ge@C_{28}**, **Sn@C_{28}** and **Pb@C_{28}**, show (Fig. 2) LUMOs with *p* orbitals over the whole surface. HOMOs have π bonding orbitals over the surface and *p* at the vertices. LUMOs and HOMOs are very similar to the singly degenerated HOMO and the triply degenerated HOMO-1 found in C_{28}^{4-}. These

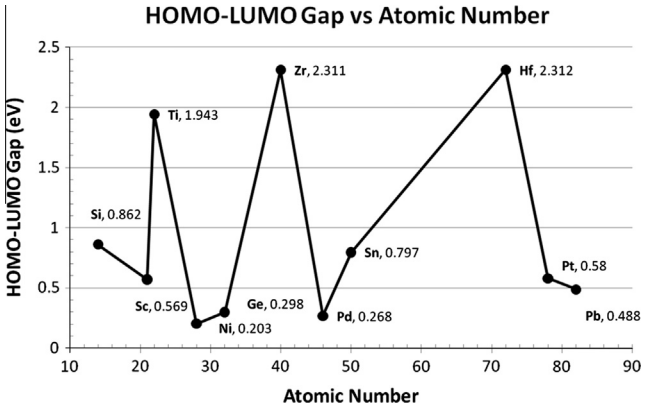

Fig. 5. HOMO–LUMO gap of all X@C_{28} in eV vs atomic number of their X species.

compounds reduced their HOMO–LUMO gap to values far from the 2.379 eV calculated for the tetraanion. Their gaps are 0.298 eV, 0.797 eV and 0.488 eV for Ge@C_{28}, Sn@C_{28} and Pb@C_{28} respectively (Fig. 5). These small values can be related to a high reactive behavior of those compounds.

Similarly to the compounds discussed above. Group-10 X@C_{28} shows orbitals that differ significantly from the tetraanion's orbitals. Per example: **Ni@C_{28}** shows (Fig. 2) LUMO, HOMO and HOMO-1 alpha and beta composed mainly of π bonds over the fullerene's surface and some *p* orbitals at vertices, with nodal planes in HOMOα and HOMO-1β that cut the Ni atom. Due to its lack of symmetry its orbitals are singly degenerated. Its HOMO–LUMO gap is calculated (Fig. 5) as 0.203 eV (which corresponds to the gap between HOMOβ and LUMOα), it is remarkably small compared with the more stable group-4 X@C_{28}. Both **Pd@C_{28}** and **Pt@C_{28}** have similar orbitals (Fig. 2). Their LUMOs, HOMOs and HOMOs-1 show mainly π bonding orbitals and *p* orbitals at the vertices on HOMOs and HOMOs-1. Their LUMOs are the doubly degenerated states 31e and their HOMOs-1 are states 30e. Both HOMOs are similar in shape (Fig. 2) to the tetraanion's HOMO and correspond to the singly degenerated state $25a_1$. These compounds have small HOMO–LUMO gaps too, with values 0.268 eV and 0.580 eV for Pd@C_{28} and Pt@C_{28} respectively (Fig. 5). The whole group can be related to high reactive compounds due to their small gaps.

Finally, **Sc@C_{28}** shows (Fig. 2) alpha orbitals that agree in shape, orbital labeling and almost in energy in comparison with Ti@C_{28} orbitals. Similarly, LUMOβ and HOMOβ match with the orbitals HOMO and HOMO-1 obtained for Ti@C_{28}. On the contrary, HOMO-1β shows π orbitals over the fullerene's surface, included its vertices and corresponds with the singly occupied state $31a_1$. Its HOMO–LUMO gap is calculated as 0.569 eV (Fig. 5), far from the 2.379 eV of C_{28}^{4-} and in agreement with the 0.306 eV calculated by Guo et al. [21]. So, the Sc@C_{28} could be highly reactive and hinders its formation.

3.5. Charge distributions and ESP maps

The experimental stability of group-4 X@C_{28} can be explained by the formation of ionic compounds $X^{4+}@C_{28}^{4-}$ that resembles the tetraanion C_{28}^{4-}. Per example: Ti@C_{28} has positive NBO and Hirshfeld charges in Ti (Table 4), with values 0.546 and 0.333 respectively. So that the C_{28}^{4-} tends to form a more stable fullerene, the compound can be understood as the ionic compound $Ti^{4+}@C_{28}^{4-}$ because their charge distributions denote a charge transfer from the endohedral atom to the cage. The charge donated by Ti is transferred preferentially to the 5:5:5 vertices, the vertex in line with Ti have NBO charge of −0.017 and Hirshfeld of −0.022 (Table 4). Similarly, all the other vertices show (Fig. 3) negative charges (Both NBO and Hirshfeld). In addition, the ESP map shows (Fig. 3) an upper hemisphere with less positive potential near the atoms compared with the lower hemisphere. In addition, both Zr@C_{28} and Hf@C_{28} have charge distributions and ESP maps very similar to that obtained for C_{28}^{4-}. According with the charge distributions and ESP map (Fig. 3), Zr@C_{28} vertices are negatively charged with the most negative charges, with values −0.094 and −0.049 for NBO and Hirshfeld analyses respectively (Table 4). In addition the vertices are regions with less positive electrostatic potential. Furthermore, similarly to Ti@C_{28}, Zr donates charge to the fullerene and it is positively charged with 1.697 according with the NBO analysis and 0.449 with Hirshfeld. In the same way, Hf@C_{28} show vertices with (Fig. 3) the most negative charges, with values −0.091 and −0.050 for NBO and Hirshfeld respectively (Table 4). This charge comes from Hf, positively charged with values 1.683 and 0.447 for NBO and Hirshfeld respectively (Table 4). Furthermore, the ESP map shows less positive regions around the vertices (Fig. 3). In line with these results, group-4 forms structures with the cation preferentially located at the center of the cage and with the most negative charges at the vertices of the tetrahedron that forms the cage. These charge distributions equilibrate more efficiently the electrostatic attraction cation-cage with the strain produced by each geometrical arrangement. The accumulation of charge at the vertices has been reported previously [22].

On the contrary, group-14 forms EFs that differ importantly from the charge distributions and ESP maps obtained for the tetraanion C_{28}^{4-}. According with the charge distribution obtained (Fig. 3), **Si@C_{28}** has its endohedral atom positively charged, with NBO charge 1.460 and Hirshfeld 0.312. Most of the charge donated by Si was transferred to the vertex in line with it, with values NBO and Hirshfeld charges of −0.185 and −0.041 (Table 4), respectively. Similarly, the ESP shows (Fig. 3) a less positive potential near the same vertex and more positive in the ring opposite to it. Both ESP and charge distributions differ slightly in comparison with that obtained for the tetraanion (Fig. 3). Also, its instability can be related with an unfavorable distribution of charge that increases the electrostatic repulsion between the cation and the most positive lower hemisphere (Fig. 3). The remaining members of group-14 locate the cation at the center. **Ge@C_{28}** shows its vertices positively charged, with values 0.064 and 0.001 according with the NBO and Hirshfeld analyses. So, the charge donated by Ge NBO 1.190 and Hirshfeld 0.444 (Table 4) was not transferred to the vertices and the vertices repel the endohedral cation. Moreover, the ESP has the most positive regions around the vertices (Fig. 3). On the contrary, **Sn@C_{28}** shows (Fig. 3) charge distributions and ESP similar to C_{28}^{4-} with a well-distributed charge over the whole fullerene coming from the endohedral Sn charged positively with 1.792 and 0.522 according with NBO and Hirshfeld respectively. In particular, the NBO distribution shows (Fig. 3) the 5:5:5 vertices with the less negative charges (with values −0.040), but, Hirshfeld and the ESP map agree with distributions very similar to that of the tetraanion. So, Sn@C_{28} resembles more to the tetraanion's charge compared with its other group members and its formation could be more suitable according with our previous observations. Finally, **Pb@C_{28}** can be compared with Ge@C_{28} because have ESP maps and NBO charge distributions very similar among them. According with the NBO distribution, Pb@C_{28} has its vertices positively charged (NBO charge 0.014) and similarly the ESP map shows (Fig. 3) regions with more positive potential near the vertices. The Hirshfeld charge distribution differs and shows the vertices negatively charged with −0.017, although the vertices are negatively charged and looks contradictious (Table 4). According with charge the distribution, the vertices are not the most negatively charged atoms and in agreement with the ESP map, neighboring atoms are most negative and have less positive electrostatic potential. In summary, Pb@C_{28} could be unstable by the same reasons of Ge@C_{28}.

Table 4
NBO and Hirshfeld charges of each endohedral atom X and the carbon vertex in line with the endohedral species of all X@C_{28}.

X@C_{28}	Vertex charge		X atom charge	
X	NBO	Hirshfeld	NBO	Hirshfeld
Si	−0.185	−0.041	1.460	0.312
Sc	−0.007	−0.032	−0.188	0.281
Ti	−0.017	−0.022	0.546	0.333
Ni	0.101	0.030	0.954	0.191
Ge	0.064	0.001	1.190	0.444
Zr	0.094	−0.049	1.697	0.449
Pd	−0.110	−0.077	0.909	0.820
Sn	−0.040	−0.040	1.792	0.522
Hf	−0.091	−0.050	1.683	0.447
Pt	−0.100	−0.071	1.134	0.577
Pb	0.014	−0.017	1.382	0.460

Similarly to the previous case, group-10 X@C_{28} produces EFs with charge distributions that differ strongly in comparison with that of group-4. In **Ni@C_{28}** the endohedral species (with NBO charge 0.954 and Hirshfeld 0.191) donates charge to the cage, but the vertex in line with Ni is positively charged with NBO charge 0.101 and Hirshfeld 0.030 (Table 4). Clearly, this represents a fact contrary to the expected behavior in that vertex, because the ESP maps near the vertices in the neutral and hollow C_{28} has the most positive values and the expected tendency is to accept charge at these points (Fig. 3). So, the charge was not transferred to the in line vertex and on the contrary the charge was transferred preferentially to its neighboring atoms and the other three vertices. Both Pd@C_{28} and Pt@C_{28} show similar charge distributions and ESP maps. **Pd@C_{28}** has carbon atom in line with Pd negatively charged, with NBO and Hirshfeld values of −0.110 and −0.077 respectively (Table 4). In addition, the Pd has a positive charge NBO of 0.909 and Hirshfeld 0.820 (Table 4). Equally important, the ESP shows (Fig. 3) the less positive regions at the vertices and the more positive potential around the hexagonal ring located below Pd. Similarly, **Pt@C_{28}** has the Pt atom positively charged (NBO 1.134 and Hirshfeld 0.577) and the vertices negatively charged with values NBO −0.100 and Hirshfeld −0.071 (Table 4). In addition, the ESP map shows the less positive potential at the vertices (Fig. 3). Although both Pd@C_{28} and Pt@C_{28} have charge distributions very similar to the C_{28}^{4-}, a close view to the ESP map reveals that the hexagonal ring located below each endohedral species has the most positive potential located differently in comparison with C_{28}^{4-} and group-4 X@C_{28} too.

Finally, **Sc@C_{28}** shows an important discrepancy between its charge distributions (Fig. 3). According with the NBO analysis, Sc does not donate charge to the fullerene and has a quite small negative charge of −0.188. In addition, the fullerene's vertices remain almost neutral, with charge −0.008. These results are not reasonable because the metallic atom (unique electropositive species in the compound) does not donate charge to the cage. On the contrary, the vertices are positively charged. In other words, the NBO charge distribution disagrees with the common sense. This problem is not showed in the Hirshfeld analysis whose charge distribution obtained a positively charged Sc (charge 0.281) surrounded by a negatively charged cage and with the most negative C atom (charge −0.032) in line with it (Table 4). Besides, the ESP map agrees with that observations it shows a more positive potential around the endohedral species and less around the vertices, especially near the vertex in line with Sc (the most negative according Hirshfeld). Altogether denotes a lack of charge accumulation at the vertices (except for the vertex in line with Sc) in order to produce a charge distribution similar to C_{28}^{4-} and group-4 X@C_{28}. As a consequence, we recommend the use of a density-based method (as Hirshfeld population analysis) in parallel with an orbital-based method in order to avoid problems with the results. Moreover, the Hirshfeld analysis agrees very well in comparison with the ESP maps in all our cases.

3.6. Aromaticity

The aromaticity plays an important role in the stabilization of the endohedral fullerenes whose cage is a fullerene that violates the IPR. While a very stable hollow fullerene as C_{60} indicate an aromatic character in its hexagonal rings and weak aromatic or antiaromatic in its pentagonal rings [16,34], the stability of many EFs whose cages are non-IPR have been explained by the donation of charge from the endohedral species to the cage, preferentially transferred to the pentagonal fused rings whose aromatic character increases. As a consequence, the stability of those non-IPR cages has been explained similarly to the stability shown by the pentalene dianion in comparison with the neutral species [3]. For that reason the following study can be related to the stability of the whole compound.

All group-4 X@C_{28} members show aromatic indexes ($NICS(0)_{iso}$ and HOMA values) which indicate an aromatic character in all their rings, this character is similar or even higher than that in case of the tetraanion C_{28}^{4-}. Table 5 lists the magnetic index $NICS(0)_{iso}$ values and the geometrical index HOMA calculated for all the non equivalent rings. (Ni@C_{28} is an exception by its C_1 symmetry group; its indices were calculated only in some rings located in similar positions). All its indices indicate an enhanced aromatic character in all its rings with the exception of the hexagonal ring opposite to Ti according with the HOMA index 0.33 less than the

Table 5
$NICS(0)_{iso}$ values (in ppm) of all X@C_{28} calculated at the center of the rings listed at the bottom. By symmetry, values in blank were omitted. $NICS(0)_{iso}$ of Ni@C_{28} were calculated only in five rings.

X	Ring 1		Ring 2		Ring 3		Ring 4		Ring 5	
	$NICS(0)_{iso}$	HOMA	$NICS(0)_{iso}$	HOMA	$NICS(0)_{iso}$	HOMA	$NICS(0)_{iso}$	HOMA	$NICS(0)_{iso}$	HOMA
Si	−6.33	0.83	−3.10	0.45	−7.60	0.59	−1.24	0.25	−13.40	−0.30
Sc	−15.97	0.85	−8.63	0.70	−7.18	0.66	−3.24	0.24	−13.44	0.25
Ti	−18.12	0.84	−16.23	0.58	−12.94	0.61	−7.32	0.59	−16.69	0.38
Ni	2.59	0.24	1.39	−0.24	10.78	−0.28	8.90	0.47	−32.09	0.33
Ge	−9.36	0.92	0.72	0.42						
Zr	−16.98	0.94	−8.27	0.68						
Pd	36.70	0.71	−21.12	0.62	77.97	−0.34	59.35	−1.05	−79.23	−4.52
Sn	−9.54	0.99	−6.11	0.52						
Hf	−16.87	0.95	−8.06	0.67						
Pt	6.32	0.75	−13.69	0.64	21.35	−0.74	−23.45	−1.84	−41.56	−7.11
Pb	−9.08	0.84	−2.68	−0.06						

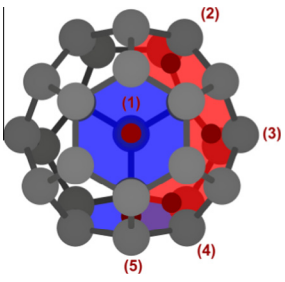

value 0.52 obtained for the hexagonal ring in the tetraanion. Anyway, its rings show full aromatic character as expected. Similarly, according with the $NICS(0)_{iso}$ and HOMA values (Table 5) $Zr@C_{28}$ and $Hf@C_{28}$ show full aromatic character in their rings. The aromatic character is increased in those rings in comparison with the tetraanion C_{28}^{4-}. The geometrical meaning of that are bond lengths more equal in their rings. The evidence suggests that the inclusion of the endohedral atom produces a local aromatic compound in addition to the global aromaticity due to the 32 π electron conjugation [17].

Unlike the previous group, Group-4 $X@C_{28}$ shows a more complex aromatic behavior. **$Si@C_{28}$** has a full aromatic character in its rings according to both indices (Table 5), $NICS(0)_{iso}$ and HOMA. With an exception, the HOMA value (−0.30) calculated for the hexagonal ring located below the Si atom denotes an antiaromatic character, contrary to the $NICS(0)_{iso}$ value −13.40 ppm which denotes a very aromatic ring. The negative HOMA index can be attributed to the decrease in symmetry that produces a hexagonal ring with shorter bond lengths 1.431 Å compared with the correspondent bond length in C_{28}^{4-} (1.446 Å). In the case of **$Ge@C_{28}$**, its HOMA values indicate an aromatic compound in all its rings. On the contrary, the positive $NICS(0)_{iso}$ value 0.72 ppm in its pentagonal rings indicate an antiaromatic character. As discussed before, the charge in this compound is not well distributed so that it does not resemble the tetraanion's distribution. The lack of charge in the vertices (shared uniquely by pentagonal rings) is not enough to produce aromatic rings. On the contrary, hexagonal rings are aromatic according with both indices. **$Sn@C_{28}$** shows a full aromatic behavior in its rings due to its all negative $NICS(0)_{iso}$ and positive HOMA values (Table 5). As has been discussed in the charge analysis, $Sn@C_{28}$ has ESP maps and charge distributions very similar to that obtained with the fully aromatic reference, the tetraanion C_{28}^{4-}. Finally, **$Pb@C_{28}$** shows a full aromatic character in its rings according with its negative $NICS(0)_{iso}$ values (−9.08 ppm and −2.68 ppm for hexagonal and pentagonal rings respectively). In addition, the HOMA index calculated for hexagonal rings has value close to 1 (0.84) that denotes an aromatic behavior. On the contrary, pentagonal rings have HOMA indices with small negative values (−0.06) that denote a weak antiaromatic or non-aromatic behavior, possibly caused by the increase in all directions of its bond lengths, contrary to the decrease shown by the 6:6 bond length in the tetraanion C_{28}^{4-} compared with its neutral form.

Finally, the calculated negative $NICS(0)_{iso}$ and positive HOMA values (Table 5) calculated for **$Sc@C_{28}$** denote an aromatic behavior in all its rings. In addition, similarly to $Zr@C_{28}$ and $Hf@C_{28}$ the $Sc@C_{28}$ has rings more aromatic in comparison with the aromatic reference C_{28}^{4-} according with their HOMA values closest to 1.

4. Conclusion

Our results compare very well with experimental results. The binding energy seems to be the best indicator of stability and in general, agrees with the abundance obtained in experiments of synthesis of group-4 $X@C_{28}$. It fails in the case of $Sc@C_{28}$, which has positive binding energy. Even though the positive binding energy is necessary, the entire stability of an endohedral C_{28} comes from the formation of an ionic compound $X^{4+}@C_{28}^{4-}$, which is fairly similar to the tetraanion C_{28}^{4-}. The charge donated from the endohedral species is accumulated mainly at the vertices where three pentagonal rings join, forming an entirely aromatic compound. As a consequence, the electrostatic potential, charge distribution, and HOMO–LUMO gap of each stable compound, resembles to that obtained for C_{28}^{4-}. Our approach agrees satisfactorily with previous knowledge and predicts the instability of several endohedral fullerenes. According with our observations we conclude that $X@C_{28}$ with endohedral group-10 atoms cannot form stable compounds. In addition, we obtained that an HOMO–LUMO gap around 2 eV produce less reactive and more stable compounds. Similarly, an aromatic behavior in all rings, and charge distribution (deeply related to the electrostatic potential) with the most negative charges at the 5:5:5 vertices are other properties observed in $X@C_{28}$ stable. In order to understand the stability in this kind of compounds and avoid incorrect predictions, their properties need to be studied in many complementary ways, independently of the method adopted.

Acknowledgements

We thank the Computing and Information Technology Division of the National Autonomous University of Mexico (UNAM) for the computer resources (assignment SC16-1-IR-64), DGAPA for funding this research under project IN102616 and CONACYT for financial support (A. Miralrio scholarship).

Appendix A. Supplementary data

Supplementary data associated with this article can be found, in the online version, at http://dx.doi.org/10.1016/j.comptc.2016.03.010. These data include MOL files and InChiKeys of the most important compounds described in this article.

References

[1] H.W. Kroto, J.R. Heath, S.C. O'Brien, R.F. Curl, R.E. Smalley, et al., C 60: buckminsterfullerene, Nature 318 (1985) 162–163.
[2] J. Heath, S. O'brien, Q. Zhang, Y. Liu, R. Curl, F. Tittel, et al., Lanthanum complexes of spheroidal carbon shells, J. Am. Chem. Soc. 107 (1985) 7779–7780.
[3] A.A. Popov, S. Yang, L. Dunsch, Endohedral fullerenes, Chem. Rev. 113 (2013) 5989–6113.
[4] M.N. Chaur, F. Melin, A.L. Ortiz, L. Echegoyen, Chemical, electrochemical, and structural properties of endohedral metallofullerenes, Angew. Chem. Int. Ed. 48 (2009) 7514–7538.
[5] L. Dunsch, S. Yang, Endohedral clusterfullerenes—playing with cluster and cage sizes, Phys. Chem. Chem. Phys. 9 (2007) 3067–3081.
[6] C.-R. Wang, T. Kai, T. Tomiyama, T. Yoshida, Y. Kobayashi, E. Nishibori, et al., Materials science: C66 fullerene encaging a scandium dimer, Nature 408 (2000) 426–427.
[7] T. Guo, M. Diener, Y. Chai, M. Alford, R. Haufler, S. McClure, et al., Uranium stabilization of C∼2∼8: a tetravalent fullerene, Science 257 (1992) 1661–1664.
[8] H.W. Kroto, D.R. Walton, Stable derivatives of small fullerenes, Chem. Phys. Lett. 214 (1993) 353–356.
[9] H. Prinzbach, A. Weiler, P. Landenberger, F. Wahl, J. Wörth, L.T. Scott, et al., Gas-phase production and photoelectron spectroscopy of the smallest fullerene, C20, Nature 407 (2000) 60–63.
[10] D.M. Cox, D.J. Trevor, K.C. Reichmann, A. Kaldor, C60La: a deflated soccer ball?, J Am. Chem. Soc. 108 (1986) 2457–2458.
[11] H. Kroto, The stability of the fullerenes Cn, with $n = 24, 28, 32, 36, 50, 60$ and 70, Nature 329 (1987) 529–531.
[12] P.W. Fowler, D. Manolopoulos, An Atlas of Fullerenes, Courier Corporation, 2007.
[13] S.-J. Zhong, C.-W. Liu, Stability of X 4 Y 24 q (X C, Si; Y B, Al, C, Si, N, P; q=- 4 to 4) and C 28 X 4 (X H, F, Cl, Br, I), J. Mol. Struct. THEOCHEM 392 (1997) 125–136.
[14] R.K. Mishra, Y.-T. Lin, S.-L. Lee, Growth mechanism of C 28 (Td) fullerene: energetics and transition-state structures analysis, Chem. Phys. Lett. 313 (1999) 437–444.
[15] B. Zhang, C. Wang, K. Ho, C. Xu, C. Chan, The geometry of small fullerene cages: C20 to C70, J. Chem. Phys. 97 (1992) 5007–5011.
[16] X. Lu, Z. Chen, Curved pi-conjugation, aromaticity, and the related chemistry of small fullerenes, Chem. Rev. 105 (2005) 3643–3696.
[17] Z. Chen, H. Jiao, A. Hirsch, W. Thiel, The 2 (N+ 1) 2 rule for spherical aromaticity: further validation, Mol. Model. Annu. 7 (2001) 161–163.
[18] O. Ori, F. Cataldo, A. Graovac, Topological ranking of C_{28} fullerenes reactivity, Fuller. Nanotub. Carbon Nanostruct. 17 (2009) 308–323, http://dx.doi.org/10.1080/15363830902782332.
[19] J.-P. Dognon, C. Clavaguéra, P. Pyykkö, A predicted organometallic series following a 32-electron principle: An@ C28 (An = Th, Pa^{+}, U^{2+}, Pu^{4+}), J. Am. Chem. Soc. 131 (2008) 238–243.
[20] X. Dai, Y. Gao, W. Jiang, Y. Lei, Z. Wang, U@C 28: the electronic structure induced by the 32-electron principle, Phys. Chem. Chem. Phys. 17 (2015) 23308–23311, http://dx.doi.org/10.1039/C5CP04127A.

[21] T. Guo, R.E. Smalley, G.E. Scuseria, Ab initio theoretical predictions of C28, C28H4, C28F4, (Ti@C28)H4, and M@C28 (M = Mg, Al, Si, S, Ca, Sc, Ti, Ge, Zr, and Sn), J. Chem. Phys. 99 (1993) 352, http://dx.doi.org/10.1063/1.465758.
[22] P.W. Dunk, N.K. Kaiser, M. Mulet-Gas, A. Rodríguez-Fortea, J.M. Poblet, H. Shinohara, et al., The smallest stable fullerene, M@C $_{28}$ (M = Ti, Zr, U): stabilization and growth from carbon vapor, J. Am. Chem. Soc. 134 (2012) 9380–9389, http://dx.doi.org/10.1021/ja302398h.
[23] R. Ahlrichs, M. Bär, M. Häser, H. Horn, C. Kölmel, Electronic structure calculations on workstation computers: the program system turbomole, Chem. Phys. Lett. 162 (1989) 165–169.
[24] F. Weigend, R. Ahlrichs, Balanced basis sets of split valence, triple zeta valence and quadruple zeta valence quality for H to Rn: design and assessment of accuracy, Phys. Chem. Chem. Phys. 7 (2005) 3297–3305.
[25] TURBOMOLE V6.5 2013, A Development of University of Karlsruhe and Forschungszentrum Karlsruhe GmbH, 1989-2007, TURBOMOLE GmbH, since 2007, n.d. Available from: <http://www.turbomole.com>.
[26] R. Dennington, T. Keith, J. Millam, et al., GaussView, version 5, Semichem Inc Shawnee Mission KS, 2009.
[27] K. Hedberg, L. Hedberg, D.S. Bethune, C. Brown, H. Dorn, R.D. Johnson, et al., Bond lengths in free molecules of buckminsterfullerene, C_{60}, from gas-phase electron diffraction, Science 254 (1991) 410–412.
[28] F. Cimpoesu, S. Ito, H. Shimotani, H. Takagi, N. Dragoe, Vibrational properties of noble gas endohedral fullerenes, Phys. Chem. Chem. Phys. 13 (2011) 9609–9615.
[29] C. Yannoni, P. Bernier, D. Bethune, G. Meijer, J. Salem, NMR determination of the bond lengths in C_{60}, J. Am. Chem. Soc. 113 (1991) 3190–3192.
[30] D.-L. Huang, P.D. Dau, H.-T. Liu, L.-S. Wang, High-resolution photoelectron imaging of cold C_{60}^- anions and accurate determination of the electron affinity of C_{60}, J. Chem. Phys. 140 (2014) 224315, http://dx.doi.org/10.1063/1.4881421.
[31] D. Muigg, P. Scheier, K. Becker, T. Märk, Measured appearance energies of fragment ions produced by electron impact on, J. Phys. B: At. Mol. Opt. Phys. 29 (1996) 5193.
[32] K. Jackson, E. Kaxiras, M.R. Pederson, Bonding of endohedral atoms in small carbon fullerenes, J. Phys. Chem. 98 (1994) 7805–7810.
[33] B. Skwara, R.W. Góra, R. Zalesny, P. Lipkowski, W. Bartkowiak, H. Reis, et al., Electronic structure, bonding, spectra, and linear and nonlinear electric properties of Ti@ C28, J. Phys. Chem. A 115 (2011) 10370–10381.
[34] M. Bühl, A. Hirsch, Spherical aromaticity of fullerenes, Chem. Rev. 101 (2001) 1153–1184, http://dx.doi.org/10.1021/cr990332q.
[35] P.J. Hay, W.R. Wadt, Ab initio effective core potentials for molecular calculations. Potentials for the transition metal atoms Sc to Hg, J. Chem. Phys. 82 (1985) 270–283.
[36] M. Frisch, G. Trucks, H. Schlegel, G. Scuseria, M. Robb, J. Cheeseman, et al., Gaussian 09, Revision D. 01; Gaussian: Wallingford, CT, USA, 2009, There No Corresp. Rec. This Ref. (n.d.).
[37] T.M. Krygowski, Crystallographic studies of inter-and intramolecular interactions reflected in aromatic character of. pi.-electron systems, J. Chem. Inform. Comput. Sci. 33 (1993) 70–78.
[38] J. Aihara, Reduced HOMO–LUMO gap as an index of kinetic stability for polycyclic aromatic hydrocarbons, J. Phys. Chem. A 103 (1999) 7487–7495.
[39] Z. Chen, H. Jiao, M. Bühl, A. Hirsch, W. Thiel, Theoretical investigation into structures and magnetic properties of smaller fullerenes and their heteroanalogues, Theor. Chem. Acc. 106 (2001) 352–363.
[40] S. Grimme, J. Antony, S. Ehrlich, H. Krieg, A consistent and accurate ab initio parametrization of density functional dispersion correction (DFT-D) for the 94 elements H-Pu, J. Chem. Phys. 132 (2010) 154104, http://dx.doi.org/10.1063/1.3382344.
[41] S. Grimme, S. Ehrlich, L. Goerigk, Effect of the damping function in dispersion corrected density functional theory, J. Comput. Chem. 32 (2011) 1456–1465, http://dx.doi.org/10.1002/jcc.21759.
[42] I. Garg, H. Sharma, N. Kapila, K. Dharamvir, V.K. Jindal, Transition metal induced magnetism in smaller fullerenes (C_n for $n \leqslant 36$), Nanoscale 3 (2011) 217–224, http://dx.doi.org/10.1039/C0NR00475H.
[43] P.W. Dunk, M. Mulet-Gas, Y. Nakanishi, N.K. Kaiser, A. Rodríguez-Fortea, H. Shinohara, et al., Bottom-up formation of endohedral mono-metallofullerenes is directed by charge transfer, Nat. Commun. 5 (2014) 5844, http://dx.doi.org/10.1038/ncomms6844.